RESEARCH ARTICLE

Elucidating the combinatorial effect of substrate stiffness and surface viscoelasticity on cellular phenotype

Daniel Chester[1,2] | Veronica Lee[1] | Paul Wagner[3] | Matthew Nordberg[1] | Matthew B. Fisher[1,2] | Ashley C. Brown[1,2]

[1]Joint Department of Biomedical Engineering, University of North Carolina at Chapel Hill and North Carolina State University, Raleigh, North Carolina, USA

[2]Comparative Medicine Institute, North Carolina State University, Raleigh, North Carolina, USA

[3]Department of Materials Science and Engineering, North Carolina State University, Raleigh, North Carolina, USA

Correspondence
Ashley C. Brown, Joint Department of Biomedical Engineering, University of North Carolina at Chapel Hill/North Carolina State University, 1001 William Moore Dr. Biomedical Partnership Center, Raleigh, NC 27607, USA.
Email: aecarso2@ncsu.edu

Abstract

Cells maintain tensional homeostasis by monitoring the mechanics of their microenvironment. In order to understand this mechanotransduction phenomenon, hydrogel materials have been developed with either controllable linear elastic or viscoelastic properties. Native biological tissues, and biomaterials used for medical purposes, often have complex mechanical properties. However, due to the difficulty in completely decoupling the elastic and viscous components of hydrogel materials, the effect of complex composite materials on cellular responses has largely gone unreported. Here, we characterize a novel composite hydrogel system capable of decoupling and individually controlling both the bulk stiffness and surface viscoelasticity of the material by combining polyacrylamide (PA) gels with microgel thin films. By taking advantage of the high degree of control over stiffness offered by PA gels and viscoelasticity, in terms of surface loss tangent, of microgel thin films, it is possible to study the influence that bulk substrate stiffness and surface loss tangent have on complex fibroblast responses, including cellular and nuclear morphology and gene expression. This material system provides a facile method for investigating cellular responses to complex material mechanics with great precision and allows for a greater understanding of cellular mechanotransduction mechanisms than previously possible through current model material platforms.

KEYWORDS
loss tangent, mechanotransduction, microgel, viscoelasticity

1 | INTRODUCTION

The homeostasis of tissues is ensured by the ability of cells to sense and respond to the changes in their mechanical and biological microenvironment. In order to better understand the mechanisms driving cellular mechanotransduction responses, many synthetic and naturally derived material platforms have been developed with varying degrees of control over material mechanics. Most studies that aim to understand cellular mechanosensing use purely elastic substrates.[1–4] These studies have shown that substrate stiffness is an important factor in modulating cell morphology and differentiation; however, results do not always mirror the cellular behavior found in vivo. This is because most tissues found in the body are not purely linearly elastic, but rather display viscoelastic properties.[5,6] To understand these discrepancies, there has been recent interest in using materials that vary material viscosity to understand its effect on cellular behavior.[7–10] Recent findings demonstrate that viscoelasticity is an important driver of cellular behavior, even when keeping the elastic component of the material constant. For

example, studies performed by Cameron et al. showed mesenchymal stem cell area, focal adhesion length, proliferation, and differentiation increased with increasing substrate loss modulus.[7]

Many hydrogel systems have had success at controlling viscoelasticity by altering the solid phase by either varying polymer and/or crosslinker molecular weight or crosslinking density.[8,9,11] However, with these material systems, the degree of control over stiffness is limited. Changing the crosslinking density not only affects the material's viscoelastic behavior, but also changes the material's elastic behavior.[12] A recent study by Cacopardo et al. investigated how altering the liquid phase of a hydrogel, through the addition of dextran molecules, affected the ability to decouple the substrate's elastic and viscous components in order to overcome the limitations associated with altering the material's polymer network.[13] While their results showed that viscoelastic properties could be controlled by adding dextran to the liquid phase, the alteration of the liquid phase did significantly change the instantaneous elastic modulus that only settled at a lower constant value after the time-dependent deformation had concluded. So far, the material systems used to study mechanosensing phenomenon have not investigated large combinatorial changes in substrate stiffness and viscoelasticity. This is largely because alterations that would change substrate stiffness would alter viscoelastic properties at the same time. However, to more fully understand the role that mechanosensing plays in maintaining homeostasis, a material system is needed that can decouple and independently control both the stiffness and viscoelasticity of the material over a wide range of physiologically relevant values. Unfortunately for systems composed of a single hydrogel material, fully decoupling the elastic and viscous components of hydrogels cannot completely happen due to the interactions between the hydrogel's liquid and solid phases.[13]

To that end, in this study we describe the characterization and use of a composite hydrogel system comprised of microgel thin films built on top of polyacrylamide (PA) gels. Microgel particles offer a high degree of control over individual particle size,[14] stiffness,[15] and functionality.[16–18] These particles can be fabricated into films through a layer-by-layer (LBL) centrifugation method to build multilayer films.[19,20] PA gels are also used to mimic soft tissues due to the high degree of control they offer over the stiffness of the resulting gel.[21] A previous study by our group has shown that once microgel particles are constructed into thin films, these films have stiffness values of ~100 kPa and have highly controllable surface loss tangent values that are capable of influencing cellular migration, morphology, and fibrotic responses.[22] However, this previous study was performed using microgel thin films built on glass. To develop a system where bulk material stiffness could also be tuned, in this study, we developed a method to build microgel thin films with controllable surface loss tangents on top of PA gels with tunable elastic moduli. Studies have shown that fibroblast cells have a mechanical depth sensing range greater than 10 μm.[23] Since the microgel thin films used in this study have a thickness of ~1.5 μm,[22] fibroblasts seeded on these films are able to sense the underlying substrate stiffness of the PA gel while also sensing the surface loss tangent value of the microgel thin film. Therefore, by combining microgel thin films with PA gels, a new material with decoupled stiffness and viscoelasticity values that can be controlled independently of one another is developed for studying the combinatory effect of both properties on cellular responses. The results presented here demonstrate the effect that changing both stiffness and viscoelasticity can have on fibroblast cells by measuring cellular and nuclear morphological changes as well as changes in gene expression in response to a wide range of these values. These results have broad implications for cellular mechanotransduction mechanisms. Additionally, this material system provides a facile method for investigating cellular responses to complex material mechanics with great precision and allow for a greater understanding of cellular mechanotransduction mechanisms than previously possible through current model material platforms.

2 | EXPERIMENTAL SECTION/METHODS

All reagents used were purchased from Sigma-Aldrich unless otherwise specified.

2.1 | Microgel particle synthesis

Microgel particles were synthesized in a precipitation-polymerization reaction and are composed of the reagents poly(N-isopropylacrylamide) (poly-NIPam), N,N′-methylenebis(acrylamide) (BIS), and Acrylic Acid (AAc). The amount of each reagent was calculated based on the percentage of each reagent of the total 140 mM final solution concentration. Sodium dodecyl sulfate (SDS) was also added to control particle size. Each reagent was then added to 95 ml of DiH$_2$O until dissolved and filtered using a 0.2 μm filter before being added to a three-necked reaction vessel. The solution was then heated to 70°C and allowed to equilibrate for 1 h. Ammonium persulfate (APS) was then dissolved in 2–3 ml of DiH$_2$O and filtered using a 0.2 μm filter before being added to the reaction vessel to initiate the reaction. The reaction was allowed to proceed for 6 h at 70°C at a stir speed of 450 RPM and then cooled overnight. The solution was filtered over glass wool to remove any large aggregates and then purified using dialysis in 1000 kDA tubing against water. Water for dialysis was changed every 12–16 h over the course of 48 h. Upon completion of dialysis, the purified solution was then freeze-dried for long-term storage at room temperature. Working solutions of 5 mg/ml were made by suspending freeze-dried particles in DiH$_2$O.

2.2 | Polyacrylamide gel fabrication

Polyacrylamide (PA) gels with stiffnesses of ~2, ~9, and ~20 kPa were made following the protocol outlined in Tse et al.[24] Amino-silanated coverslips were prepared by adding 300 μl of 0.1 M NaOH to 25-mm coverslips and allowing them to dry overnight. Once dry, a uniform layer of NaOH formed on the glass; the coverslips were swabbed with (3-aminopropyl)triethoxysilane (APTMS) and allowed to react for 5 min. The coverslips were then rinsed with DiH$_2$O to remove any unreacted APTMS, then submerged in a solution of 0.5%

glutaraldehyde in PBS for 30 min. The coverslips were then removed and allowed to dry. Separately, chloro-silanted coverslips were made by spreading 100 μl of dichlorodimethylsilane (DCDMS) onto each coverslip and allowed to react for 5 min before being washed with DiH$_2$O. Acrylamide and bis-acrylamide were mixed to the required concentrations in DiH$_2$O. The specific ratios of percent acrylamide to percent bis-acrylamide were as follows: 2kPa: 5:0.06; 9 kPa: 5:0.3; 20 kPa: 8: 0.264. A 1/100 total volume solution of 10% w/v of APS and a 1/1000 total volume of tetramethylethylenediamine (TEMED) was added to the mixture and vortexed to ensure uniform mixing. 25 μl of the unpolymerized gel solution was then pipetted onto the amino-silanted coverslips and a chloro-silanated coverslip was placed on top. The gel solution was allowed to polymerize at room temperature for 30 min. After polymerization, the gels were submerged in PBS and the chloro-silanated coverslips removed.

2.3 | Composite microgel film and polyacrylamide gel substrate formation

To build microgel thin films on top of PA gels, the PA gels were first functionalized with sulfosuccinimidyl-6-(4′-azido-2′-nitrophenylamino)-hexanoate (sulfo-SANPAH). A 0.2 mg/ml solution of sulfo-SANPAH was made and 500 μl was added to each PA gel. The gel was then placed in a 365-nm UV light source and exposed for 10 min. The gels were removed from the UV source and rinsed with PBS for 5 min while shaking before repeating the exposure to UV light a second time. PA gels were washed again and a 0.05 monomolar solution of linear poly-ethyleneimine (PEI) was added. The films were then incubated at 4°C overnight. Following incubation, the first layer of microgels was built on the PA gel by adding a 0.1 mg/ml solution of microgels to the PA gels and centrifuging at 3700 RPM for 10 min. To increase the stability of the multilayer film built on the PA gel, the first layer of microgels is crosslinked to the PEI via a solution of 2 mM 1-ethyl-3-(3-dimethylaminopropyl) carbodiimide (EDC) and 5 mM N-hydroxysuccinimide (NHS) in a 0.1 M solution of 2-ethanesulfonic acid (MES) pH 4.7. After crosslinking, the film was submerged in the PEI solution for 30 min and a second layer was built. This process was then repeated until there were four layers of microgel particles. The microgel film was then left un-crosslinked or was crosslinked using concentrations of 0.2 mM/0.5 mM, 2 mM/5 mM, or 20 mM/50 mM of EDC/NHS. The completed films were then coated in rat tail collagen I at a concentration of 40 μg/ml and incubated overnight at 4°C.

2.4 | Mathematical modeling

The microgel and PA gel system was modeled in one dimension as a system of two springs in series (Figure S2A). The materials were modeled as linear elastic, homogenous (within each layer) materials. For the PA gel layer, the assumption of no viscoelasticity is valid based on prior literature.[24] Although the microgel layer is viscoelastic,

by modeling several elastic stiffness values, the range of stiffness values, which may occur even following stress relaxation, can be covered. Each layer has an associated stiffness (k) or elastic modulus (E) along with a length. The cross-sectional area (A) is arbitrary. For a given applied force (F), the equation for each layer is

$$F_{\text{layer}} = k_{\text{layer}} \times \Delta\ell_{\text{layer}}, \tag{1}$$

where $\Delta\ell$ is the change in length. The overall composite follows a similar structure of

$$F_{\text{comp}} = k_{\text{comp}} \times \Delta\ell_{\text{comp}}. \tag{2}$$

Since the springs are in series,

$$\ell_{\text{layer}} = \ell_{\mu\text{gel}} + \ell_{\text{PA gel}}, \tag{3a}$$

$$\Delta\ell_{\text{layer}} = \Delta\ell_{\mu\text{gel}} + \Delta\ell_{\text{PA gel}}. \tag{3b}$$

Substituting Equations 1 and 2 into Equation 3 gives

$$\frac{F_{\text{comp}}}{k_{\text{comp}}} = \frac{F_{\mu\text{gel}}}{k_{\mu\text{gel}}} + \frac{F_{\text{PA gel}}}{k_{\text{PA gel}}}. \tag{4}$$

Since the force is the same in each layer and the composite, this simplifies to

$$\frac{1}{k_{\text{comp}}} = \frac{1}{k_{\mu\text{gel}}} + \frac{1}{k_{\text{PA gel}}}, \tag{5a}$$

or,

$$k_{\text{comp}} = \frac{k_{\mu\text{gel}} \times k_{\text{PA gel}}}{k_{\mu\text{gel}} + k_{\text{PA gel}}} \tag{5b}$$

To convert stiffness to elastic modulus, 1-D formulations of stress, strain, and their relationship are used:

$$\sigma = \frac{F}{A}, \tag{6a}$$

$$\varepsilon = \frac{\Delta\ell}{\ell}, \tag{6b}$$

$$\sigma = E \times \varepsilon. \tag{6c}$$

Substituting Equation 1 and 2 into Equation 6a, and Equation 6a and 6b into Equation 6c yields

$$k_{\text{layer}} = \frac{E_{\text{layer} \times A}}{\ell_{\text{layer}}}, \tag{7a}$$

$$k_{\text{comp}} = \frac{E_{\text{comp} \times A}}{\ell_{\text{comp}}}, \tag{7b}$$

after rearranging to solve for *k*. Substituting Equations 7a and 7b into Equations 5a and 5b yields

$$\frac{\ell_{comp}}{E_{comp}} = \frac{\ell_{\mu gel}}{E_{\mu gel}} + \frac{\ell_{PA\,gel}}{E_{PA\,gel}},\qquad(8a)$$

$$E_{comp} = \frac{\ell_{comp}}{\frac{\ell_{\mu gel}}{E_{\mu gel}} + \frac{\ell_{PA\,gel}}{E_{PA\,gel}}}.\qquad(8b)$$

Parameter values are summarized in Table S1.

2.5 | Loss tangent characterization

To characterize how the surface loss tangent of the microgel films changed with crosslinking, loss tangent imaging was performed using a Cypher ES AFM (Asylum) and pyramidal BL-AC40TS-C2 cantilevers (Olympus) with a cantilever constant of 0.09 N/m. 20×20 μm areas were measured in three different locations on two different batches of microgel films built on glass for each condition.

2.6 | Cell membrane staining and seeding

Prior to seeding, cells were stained with a CellBrite fix membrane dye (Biotium). 20 μl of a 100x solution of the membrane dye was added to ~1,000,000 human dermal neonatal fibroblasts (HDFn) resuspended in PBS. The cells were allowed to incubate in the membrane dye at 37°C for 15 min before being mixed by gently pipetting and then incubating again for another 15 min at 37°C. HDFns were then seeded at a concentration of 15 k cells per well on the PA gel and microgel film constructs following collagen I coating and incubated at 37°C for 24 h. After 24 h the cells were fixed in a solution of 95% absolute methanol and 5% acetic acid for 5 min at −20°C. After fixing, cells were incubated for 30 min with NucBlue (ThermoFisher Scientific), which is a high purity form of the classic DAPI stain in a room temperature-stable solution, in PBS to visualize the nucleus.

After fixation and cell staining, samples were mounted onto glass microscope slides using Flouromount-G (Thermo Fisher). Samples were then imaged using an EVOS FL Auto (Thermo Fisher) and a scale bar added to each image. Cell area, cell circularity, nuclear area, nuclear circularity, and nuclear aspect ratio were then measured in ImageJ for approximately 30 cells per condition. To measure cell or nuclear area and circularity, the perimeter of the cell or nucleus was traced using the freehand area selection tool. ImageJ was then used to calculate cell area and cell circularity for whole cell measurements or nuclear area, circularity, and nuclear aspect ratio for nuclear measurements. Circularity is calculated as 4π (area/perimeter^2). Because cell shape and size change dramatically during cell division, any cells that had multiple nuclei in the cell body were excluded from analysis. Cell attachment was also determined for images by counting the number of cells per image for at least three images per sample and four samples per condition. Average cell number was determined per unit area.

2.7 | Real time quantitative polymerase chain reaction gene expression

Cell lysis and RNA purification was performed following the manufacturer protocol using a Quick-RNA Microprep Kit (Zymo Research). Using this kit, cells were lysed in a lysis buffer, cleared through a column, purified through a series of washes and a DNase digestion, and eluted with DNase/RNase-free water into a microcentrifuge tube. RNA sample purity, quality, and concentration were then measured using a Nanodrop (Thermo Fisher). cDNA synthesis and amplification was then performed following the manufacturer protocol using a GoScript™ Reverse Transcriptase kit (Promega). After completion of cDNA synthesis and amplification, purity, quality, and concentration was measured using a Nanodrop. Real time quantitative polymerase chain reaction (RT-qPCR) was performed by following the manufacturer protocol using SYBR™ Select Master Mix (Applied Biosystems). The housekeeping gene used for this study was GAPDH and the two genes of interest used in this study encoded for alpha-smooth muscle actin (α-SMA) and connective tissue growth factor (CTGF). Specific Primer IDs and sequences can be found in Table S2. Primers for the house keeping genes and genes of interest were custom ordered from Thermo Fisher. Three samples for each condition were then pipetted, in duplicate, into a 96-well PCR plate, sealed to prevent evaporation or contamination due to condensation, and placed in a QuantStudi 3 real-time PCR system (Thermo Fisher). Samples were then heated to 70°C for 15 min, cooled to 50°C for 2 min, heated to 95°C for 2 min, and then for 40 cycles the samples were heated to 95°C for 15 s, cooled to 60°C for 1 min, and a data point taken after the completion of 1 min at 60°C. Relative gene expression was measured by calculating the $\log_{10}(2^{-\Delta\Delta CT})$ values for each sample. The $\log_{10}(2^{-\Delta\Delta CT})$ were then normalized to a microgel film with a surface loss tangent value of 0.70 built on a glass coverslip in order to compare the gene expression results.

2.8 | MatLab 3D graph modeling

To visualize the trends occurring across both stiffness and loss tangent, 3D graphs of the data were created using MatLab. In MatLab, the data was compiled into matrices and a cubic spline interpolation was used to create 3D surfaces of the data. Since microgel film surface loss tangent, PA gel substrate stiffness, and the measured cellular responses are all continuous variables, a cubic spline interpolation was used to model the relationships between them.[25]

2.9 | Statistical analysis

All statistical analysis was performed in the Prism software (Graphpad). Linear regression was performed for loss tangent values as a function of film crosslinking conditions; specifics of the linear regression analysis are presented in Table S3. Data was statistically analyzed using either a one-way or two-way ANOVA with subgroup

comparisons done using the Tukey post-hoc test at a 95% confidence interval. For two-way ANOVA analyses, comparisons between mean values by gel stiffness and mean values by film loss tangent are presented in Tables S4–S11. All results are reported as the mean ± the standard deviation.

3 | RESULTS

3.1 | Microgel thin film viscoelasticity at varying external crosslinking densities

We first synthesized poly(N-isopropylacrylamide) (poly-NIPam) microgels copolymerized with Acrylic Acid (AAc) and crosslinked with varying amounts of N,N′-methylenebis(acrylamide) (BIS). Particles were then fabricated into four layer films constructed on sulfosuccinimidyl-6-(4′-azido-2′-nitrophenylamino)-hexanoate (sulfo-SANPAH) functionalized PA gels of varying stiffness or glass controls using a LBL method alternating layers of microgels and polyethyleneimine (PEI). To increase the stability of the multilayer film built on the PA gel, the first layer of microgels is crosslinked to the PEI via a solution of 2 mM 1-ethyl-3-(3-dimethylaminopropyl) carbodiimide (EDC) and 5 mM N-hydroxysuccinimide (NHS).

We first sought to characterize how varying the level of internal particle crosslinking (i.e. BIS percentage) and EDC/NHS crosslinking of films influenced film loss tangent parameters. A previous study by our lab showed that increased intraparticle BIS crosslinking decreases the viscoelastic nature of microgel thin films as observed by decreased film surface loss tangent.[22] BIS crosslinking occurs during microgel particle synthesis, therefore, internally within the particle. However, external crosslinking can also be performed by utilizing EDC and NHS coupling chemistry to crosslink the carboxyl groups found in the AAc within the particle to the amine groups found in the PEI that diffuses in and out of the microgel particles and between layers.[26,27] In the absence of external crosslinking, changing the internal crosslinking density by altering the amount of BIS used during particle polymerization was enough to change film surface loss tangent in a linear fashion where increasing the amount of internal crosslinking resulted in lower surface loss tangent values. This is due to the decrease in polymer mobility caused by the increase in the internal crosslinking density.

External crosslinking can further change the viscoelastic nature of microgel thin films and was investigated by creating 4-layer thin films on glass with microgel particles that had either 1%, 2%, 4%, or 7% BIS crosslinking and were then either externally crosslinked with a solution containing 0 mM/0 mM, 0.2 mM/0.5 mM, 2 mM/5 mM, or 20 mM/50 mM EDC/NHS (Figure 1B). Results showed that as external EDC/NHS crosslinking increased, the viscoelastic nature of the films normalized to a minimum surface loss tangent value of ~0.6 (Figure 1C). The results indicate that externally crosslinking the microgel films has a significantly greater effect on microgel film loss tangent than does internally crosslinking the particles during synthesis. Even at a low external crosslinking condition of 0.2 mM EDC/0.5 mM NHS, the loss tangent values significantly decreased on films that had high

loss tangent values in the absence of external crosslinking for all conditions except the 7% BIS particle films. For 1% BIS films, loss tangent was significantly decreased ($p < .001$) for all crosslinking conditions compared to uncrosslinked films and was also significantly decreased ($p < .001$) between 0.2 mM EDC and 2 mM EDC groups. For 2% BIS films, loss tangent was significantly decreased ($p < .001$) for all crosslinking conditions compared to uncrosslinked films and was also significantly decreased between 0.2 mM EDC and 2 mM EDC groups ($p < .001$) and 0.2 mM EDC and 20 mM EDC groups (0.01). For 4% BIS films, loss tangent was significantly decreased ($p < .001$) for all crosslinking conditions compared to uncrosslinked films. The normalization of the microgel film surface loss tangent values at higher external crosslinking densities also suggests that the polymer chains were fully immobilized. Linear regression was run to determine the relationship between loss tangent values and crosslinking conditions; trend lines are shown in Figure 1C and equations are presented in Table S3.

To ensure that changing the underlying substrate did not change the resulting surface loss tangent value of microgel thin film, 4-layer films were built upon PA gels with a stiffness of 9 kPa and crosslinked externally in a solution of 2 mM EDC/5 mM NHS. Loss tangent imaging of the films built on PA gels did not show any statistical significance when compared to the values measured of the same types of films built on glass (Figure S1). Furthermore, to determine the contribution of the microgel thin film layer to the composite stiffness values, we developed a simple, 1-D mathematical model of the composite system (Figures S2A). Effective stiffness (k_{comp}) and modulus (E_{comp}) is plotted as a function $k_{PA\,gel}$ and $E_{PA\,gel}$, respectively, in Figure S2B with % error plotted as a function $k_{PA\,gel}$ and $E_{PA\,gel}$, respectively, in Figure S2C. Overall, for all values of $k_{PA\,gel}$ and $E_{PA\,gel}$, composite values were very close to the values for the PA gel layer, as expected. Percent error increased as values of $k_{PA\,gel}$ and $E_{PA\,gel}$ increased. For $k_{PA\,gel}$, percent error at microgel stiffness of 2353, 1059, and 235 N/μm (corresponding to moduli of 2353, 1059, and 235 N/μm) was 0.3%, 1.5%, and 3.2%, respectively. For $E_{PA\,gel}$, percent error at microgel moduli of 2, 9, and 20 kPa was 17.3%, 15.9%, and 13.9%, respectively. Since the PA gel modulus of 20 kPa represents the highest possible value among the groups tested, these data show that the elastic stiffness and modulus of the composite gels were largely dictated by the underlying PA gel layer, and that differences between different PA gel groups were maintained even when tested as a composite with the microgel layer.

3.2 | Quantification of fibroblast morphology

To analyze the influence that both substrate stiffness and surface viscoelasticity have on cell morphology, microgel films of different surface loss tangent values built on PA gels of different stiffnesses were coated with collagen. Human dermal fibroblasts (HDFns) were then seeded on all of the collagen coated microgel films and imaged after 24 h. Images were processed in ImageJ to quantify cell area and cell circularity. Cells seeded on microgel thin films built on 2, 9, and 20 kPa (Figure 2, Figures S3, S4) all showed similar trends in cell area
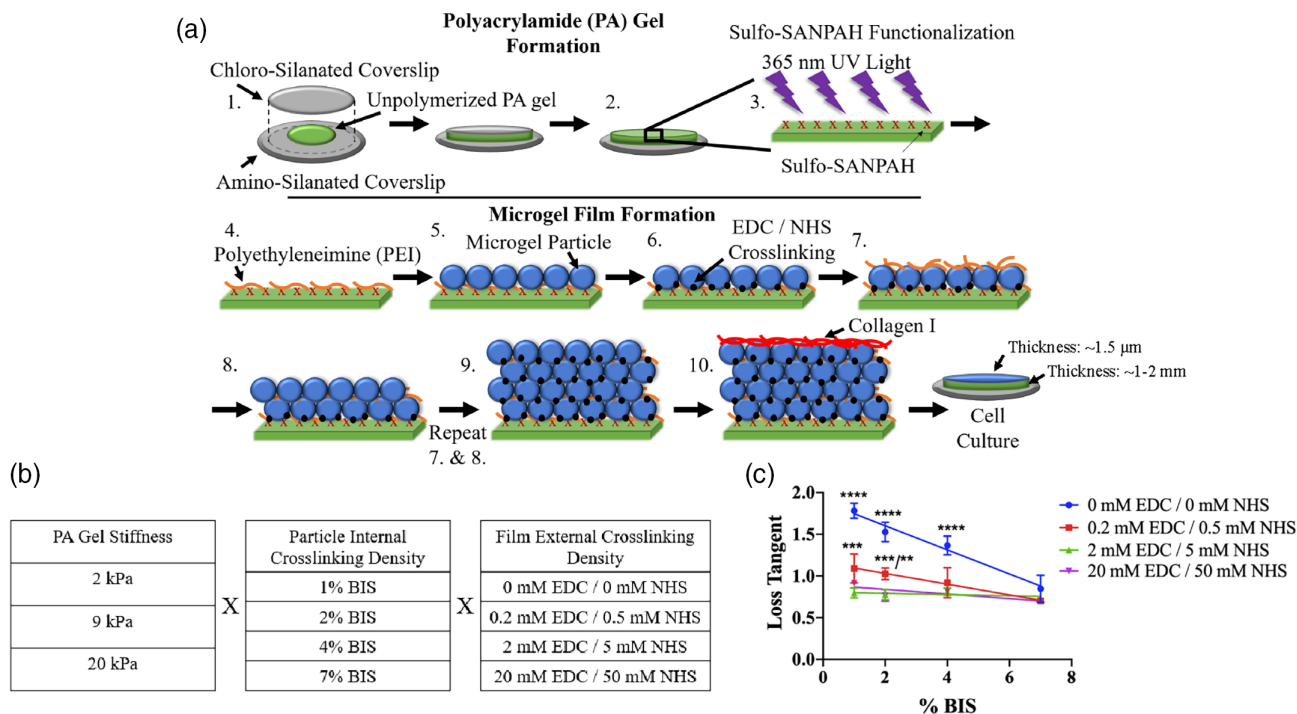
FIGURE 1 Polyacrylamide (PA) gel and microgel composite substrate synthesis and characterization: (a) Composite microgel and PA gel substrates were created by first polymerizing a PA gel on a glass coverslip. The polymerized PA gel was functionalized with sulfo-SANPAH and incubated with polyethyleneimine for microgel film buildup. Microgel film buildup occurred in a layer-by-layer fashion with ethyl-3-(3-dimethylaminopropyl) carbodiimide/N-hydroxysuccinimide crosslinking occurring after the first layer and again after the fourth layer. (b) A chart of the PA gel stiffnesses, microgel particle internal crosslinking densities, and different amounts of external film crosslinking concentrations used to create the composite substrates. (c) Loss tangent AFM imaging was performed on three different locations on two different microgel films built on glass to measure how external crosslinking influences films viscoelasticity. Results are shown as the mean ± standard deviation. As external crosslinking increased, the loss tangent of the microgel films decreased as does the viscoelastic nature of the film. Significant differences were measured between films with different external crosslinking concentrations, but the same percentage of N,N′-methylenebis(acrylamide). ** $p < .01$, *** $p < .001$, **** $p < .0001$

and circularity for surface loss tangent values greater than 1. At surface loss tangent values greater than 1, cell area decreased and cell circularity increased as the surface loss tangent increased with the highest cell areas corresponding to cells seeded on the stiffest PA gels. However, at surface loss tangent values lower than 1, the cell morphologies measured across all conditions were highly variable and seemed to oscillate between high and low area and circularity values of 500–3000 μm^2 and 0.2–0.8, respectively.

Further indicating the importance of the threshold loss tangent value of ~1, plotting the data by substrate stiffness instead of the surface loss tangent (Figure 3) showed similar trends as when the data was plotted by the surface loss tangent. Around the threshold loss tangent value of 1, substrate stiffness caused a linear increase in cellular area as seen by the data measured at the surface loss tangent value of 1.09. At a loss tangent value greater than 1, cell area did not appear to change with substrate stiffness as seen by the data measured at the surface loss tangent value of 1.53. At loss tangent values less than 1, the effect of substrate stiffness on cellular area was again variable as cells seeded on the surface loss tangent value of 0.81 did not seem to have their area effected by substrate stiffness while cells seeded on the surface loss tangent value of 0.68 saw

a linear increase in cellular area with substrate stiffness. When cells were seeded on PA gels alone without any films, area increased linearly and circularity decreased linearly with increasing PA gel stiffness (Figure S5). We additionally evaluated the influence of loss tangent and stiffness on cell attachment. We found that cell attachment was roughly equivalent on most surfaces studies (Figure S6, Table S6); however, attachment was significantly greater on 20 kPa gels with 0.81 loss tangent films compared to 1.53 loss tangent films ($p < .01$), on 20 kPa gels with 0.81 loss tangent films compared to 2 kPa gels with 0.81 loss tangent films ($p < .01$), and 9 kPa gels with 1.53 loss tangent films compared to 2 kPa gels with 1.53 loss tangent films ($p < .05$).

To better visualize the trends of cell morphology across both stiffness and viscoelasticity, results were also plotted in 3D (Figure 4). The 3D plots allow for more clear visualization that the trends across the surface loss tangent are maintained on the different PA gel stiffness and only the magnitude of the cell area increases as stiffness increases. The variability at a surface loss tangent lower than 1 can be observed by the frequent rise and fall of the surface at those values, while the surface remains relatively smooth on surface loss tangent values greater than 1.
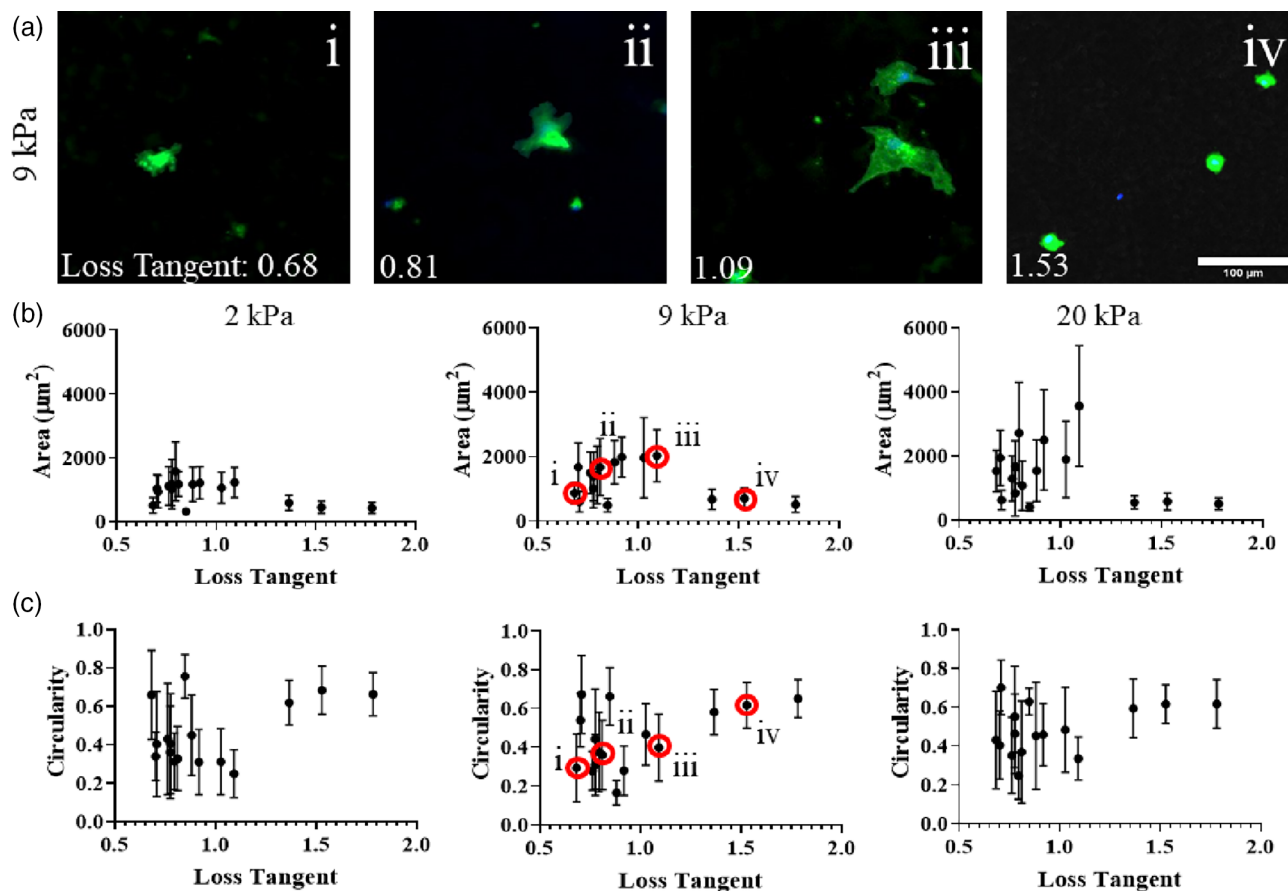
FIGURE 2 Cellular morphology with varying microgel film surface loss tangent: images were taken 24 h after seeding human dermal neonatal fibroblasts (HDFn) cells on collagen coated composite substrates with a polyacrylamide (PA) gel stiffness of either 2, 9, or 20 kPa and microgel film surface loss tangent values ranging from 0.6–1.8. (a) Representative images (i–iv) of HDFn cells seeded on a composite substrate with a 9 kPa PA gel stiffness and microgel surface loss tangent of 0.68, 0.81, 1.09, and 1.53, respectively. The images were analyzed in ImageJ to measure cellular area (b) and cellular circularity (c) with at least 30 cells measured across three different composite substrates. Results show a trend with loss tangent where, irrespective of the substrate stiffness, at loss tangents greater than 1 there is a decreasing trend in cellular area and an increasing trend in cellular circularity. However, at loss tangent values lower than 1, the response becomes highly variable

3.3 | Quantification of fibroblast nucleus morphology

The nucleus plays an important role in cellular mechanotransduction processes.[28] To elucidate the role that both substrate stiffness and surface loss tangent have on nucleus morphology, the area, circularity, and aspect ratio of HDFn nuclei were analyzed in ImageJ 24 h after seeding on a subset of collagen coated microgel/PA gel substrates (Figure 5; Figure S7). Similar to cell morphology, nuclear morphology across microgel film surface loss tangent follows similar trends across different PA gel stiffnesses. Nucleus area and aspect ratio increased until a microgel film surface loss tangent of approximately 1. At surface loss tangent values lower than 1, nucleus area and aspect ratio have a higher degree of variability and oscillate between high and low values of 100–200 μm^2 and 1–3, respectively. Nucleus circularity decreased to a value between 0.7–0.8 as microgel film surface loss tangent decreased to a value of 1 and began to oscillate between circularity values of 0.6–0.9 on microgel films with surface loss tangent values lower than 1 irrespective of PA gel stiffness. To better visualize

the nuclear morphology trends across both stiffness and surface loss tangent, these values were also plotted in 3D (Figure 6). On these graphs, similar to the graphs depicting cellular morphology, nuclear morphology appears to follow a consistent trend along loss tangent and the magnitude of the observed responses increase with substrate stiffness. Additionally, nuclear morphology has a similar trend of increased variability at surface loss tangent values less than 1 as observed with cellular morphology.

3.4 | Real time quantitative PCR gene expression

Changes in substrate mechanics and nuclear morphology have been linked to changes in pro-fibrotic gene expression. To determine the effects that both substrate stiffness and surface viscoelasticity had on fibroblast gene expression, RT-qPCR was performed to quantify α-SMA (Figure 7A, C) and CTGF expression (Figure 7B, D) in HDFn cells seeded on composite substrates for 24 h. Results showed that substrate stiffness influenced the overall magnitude of the relative
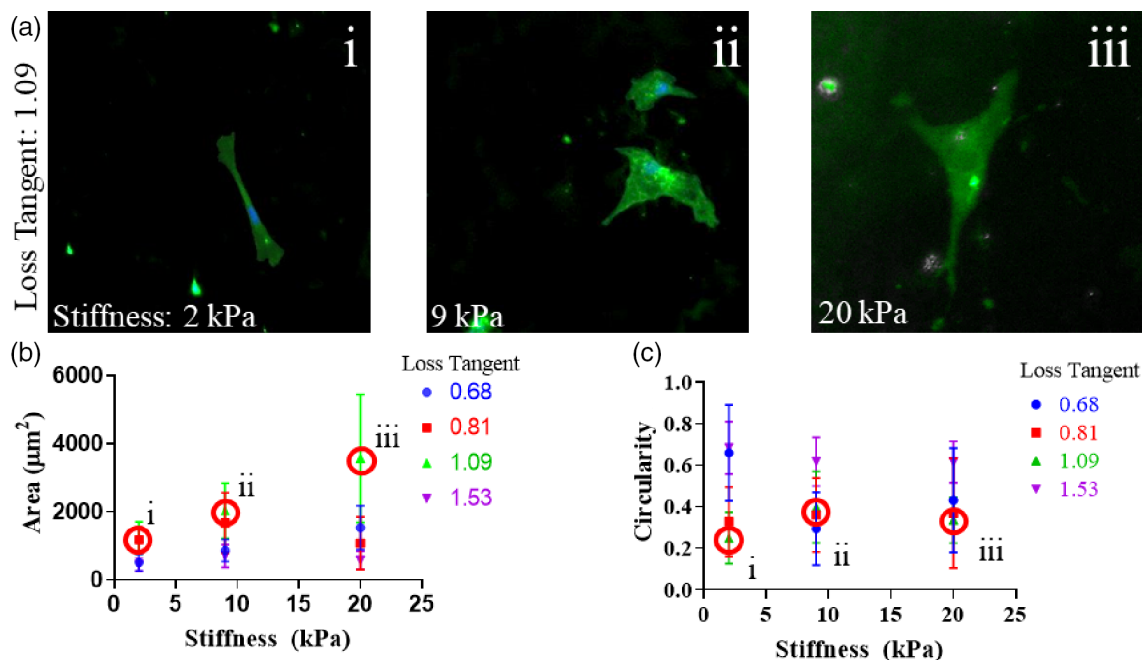
FIGURE 3 Cellular morphology with varying polyacrylamide (PA) gel stiffness: Images were taken 24 h after seeding human dermal neonatal fibroblasts (HDFn) cells on collagen coated composite substrates with a PA gel stiffness of either 2, 9, or 20 kPa and microgel film surface loss tangent values ranging from 0.6–1.8. (a) Representative images (i–iii) of HDFn cells seeded on a composite substrate with a microgel film surface loss tangent of 1.09 and a PA gel stiffness of 2, 9, or 20 kPa, respectively. The images were analyzed in ImageJ to measure cellular area (b) and cellular circularity (c) with at least 30 cells measured across three different composite substrates. Results show that for cellular area, substrate stiffness had the biggest impact at a loss tangent value of 1.09. However, PA gel stiffness did not seem to have as great of an effect on cellular circularity
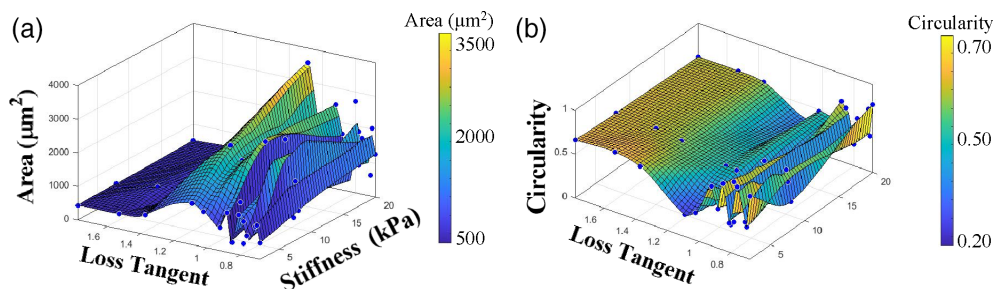

FIGURE 4 Cell morphology responses to changing loss tangent and Stiffness: To better visualize the trends in cellular morphology across both stiffness and loss tangent, the area (a) and circularity (b) responses of human dermal neonatal fibroblasts cells were plotted in 3D. These graphs show that cell morphology responses follow similar trends as dictated by the loss tangent and that the magnitude of the observed responses changes with stiffness. These graphs also highlight the variability in observed responses seen on substrates with loss tangent values below 1

rates of expression when normalized to the lowest surface loss tangent condition built on glass coverslips. For α-SMA expression, cells seeded on 20 kPa substrates had the highest overall rates of expression with values seen to be ~1.5–2 times that of the control, followed by cells seeded on 2 kPa substrates with values ~0.5–1 times higher than the control. The lowest rates of expression were seen from cells seeded on 9 kPa substrates with values of ~1 times lower than the control. For CTGF expression, cells seeded on 2 and 20 kPa substrates had the highest overall rates of expression with values seen to be ~0.5 times that of the control while cells seeded on the 9 kPa substrates had the lowest rates of expression with values ~0.5 times lower than the control. Results also showed that the surface loss

tangent values mediated trends in α-SMA expression. With α-SMA expression, the intermediate surface loss tangent values of 0.81 or 1.09 had the lowest rates of expression and created a non-monotonic response pattern. However, surface loss tangent did not seem to elicit any significant changes overall in CTGF expression.

4 | DISCUSSION

In this study, we demonstrate the ability to easily create a composite substrate in which both the surface viscoelasticity and bulk stiffness can be controlled to facilitate the study of the combinatory effect
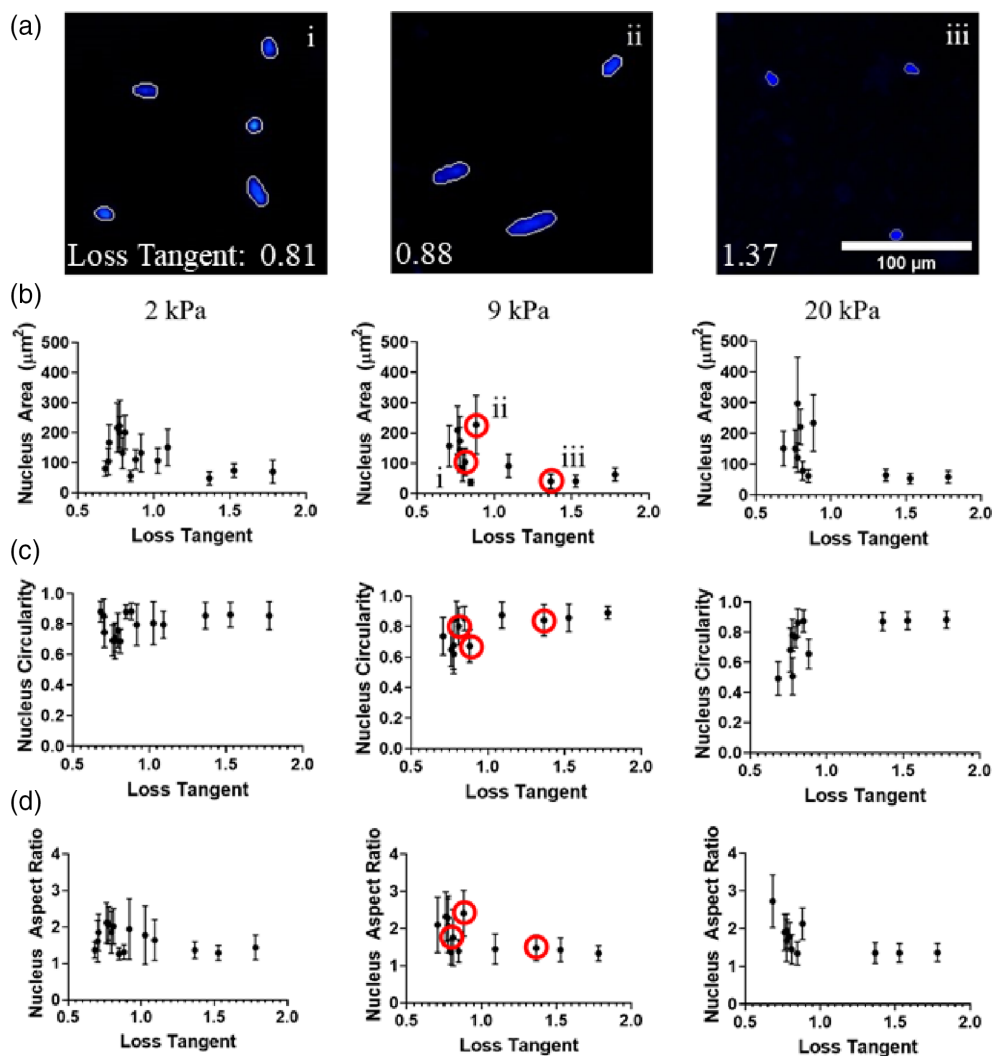
FIGURE 5 Nuclear morphology changes across changing substrate stiffness and viscoelasticity: human dermal neonatal fibroblasts cells were seeded on collagen coated composite substrates and imaged after 24 h. (a) Representative images of nuclear morphology on 9 kPa PA gels with the pictures labeled i–iii corresponding to the points circled in red on the corresponding graphs. Nuclear morphology was then characterized by measuring nucleus area (b), circularity (c), and aspect ratio (d) in ImageJ. At least 30 cells were measured across three different composite substrates. Similar to cellular morphology, nuclear morphology trends were dictated by substrate loss tangent however, it does not appear that substrate stiffness influenced the magnitude of the observed responses
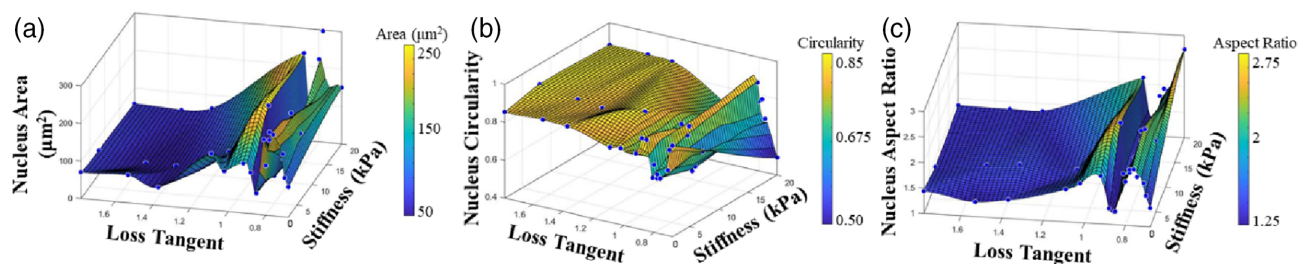

FIGURE 6 Cell nucleus morphology responses to changing loss tangent and stiffness: to better visualize the trends in nuclear morphology across both stiffness and loss tangent, the area (a), circularity (b), and (c) aspect ratio responses of human dermal neonatal fibroblasts cells were plotted in 3D. These graphs show that nucleus morphology responses follow similar trends, as dictated by the loss tangent, and that the magnitude of the observed responses changes with stiffness. These graphs also highlight the variability in observed responses seen on substrates with loss tangent values below 1

these mechanical properties have on cellular and nuclear morphology. Surface viscoelasticity was controlled by using microgel thin films with different internal and external crosslinking densities while substrate stiffness was controlled by changing the amounts of acrylamide and bis-acrylamide used during PA gel polymerization. Microgel thin films have a thickness of ~1.5 μm and fibroblasts have been shown to have

the ability to sense the mechanics of an underlying substrate to a depth of 10–20 μm.[22,29] This ensures that both the viscoelasticity of the microgel films and the stiffness of the PA gels is within the sensing capabilities of the HDFn cells used in this study. Furthermore, our modeling results demonstrate that the stiffness sensed by the cells is dominated by the PA gels with minimal contribution from the microgel
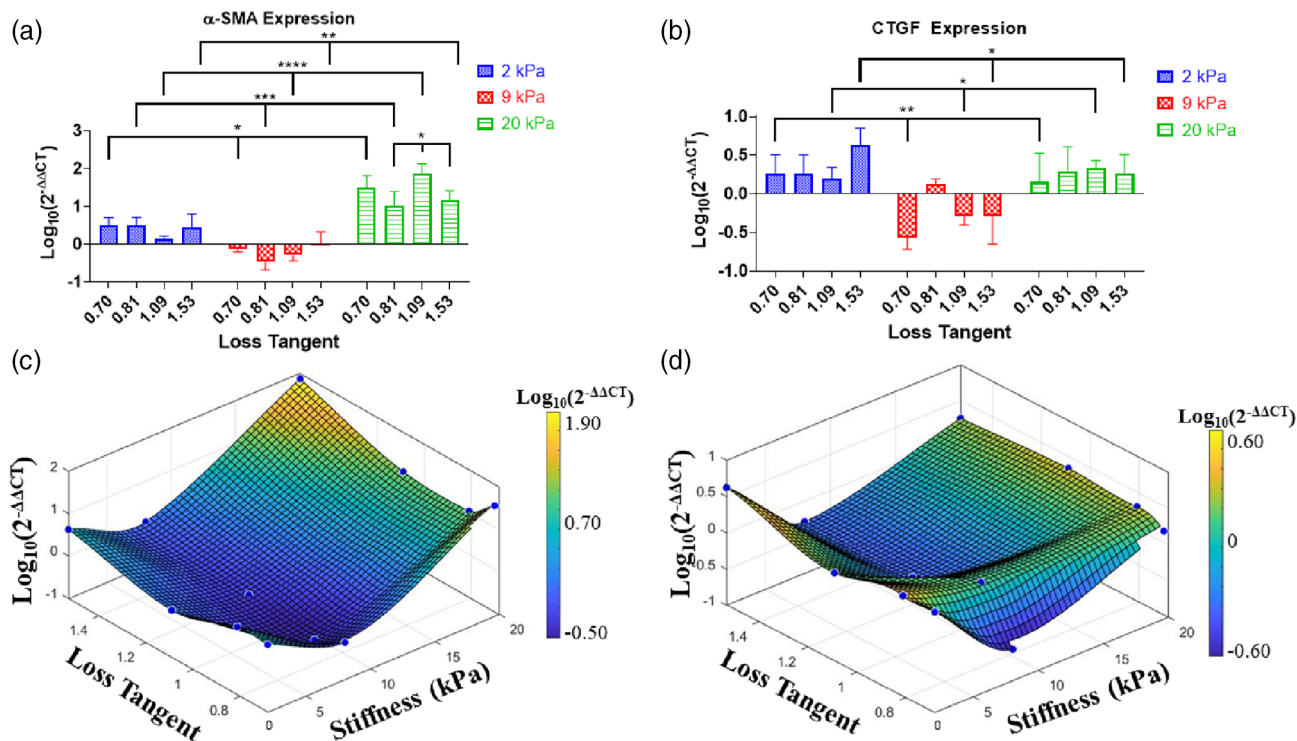
FIGURE 7 Alpha-smooth muscle actin (α-SMA) and connective tissue growth factor (CTGF) gene expression across changing loss tangent and stiffness: Gene expression of α-SMA (a) and CTGF (b) was measured by real time quantitative polymerase chain reaction. The values were also plotted in 3D to better visualize how α-SMA (c) and CTGF (d) gene expression changed across both stiffness and loss tangent. The trends shown on the 3D graphs show that substrate stiffness directs cellular gene expression while loss tangent does not seem to have a significant effect

thin films. These results provide new context for prior reports investigating the role of substrate stiffness in directing cell and nuclear morphology changes and alterations in gene expression when cells are cultured on PA gels with controllable linear elastic stiffness. We showed, as many prior studies on PA gels only conditions have, that cell spreading increases and cell circularity decreases with increasing gel stiffness (Figure S6). Additionally, it has been previously reported that nuclear area increases[30] and nuclear circularity decreases[31] in response to increasing substrate stiffness, and α-SMA[32] and CTGF expression[33] also increase with increasing substrate stiffness on traditional PA gels. Our results demonstrate that altering the loss tangent of the PA gel surface influences cellular outcomes.

Analysis of cell morphology on substrates with varying stiffness and viscoelasticity showed that microgel film surface loss tangent was crucial for directing the trends of the response observed while PA gel stiffness directed the magnitude of the response observed. As substrate stiffness increased, the magnitude of the cell area generally increased as well. The increase in magnitude of cell area as substrate stiffness increases is consistent with studies performed on purely elastic materials where an increase in cell area is observed as substrate stiffness increases.[4,34,35] However, regardless of the stiffness of the PA gel, cells had a different trend of responses depending on the viscoelasticity of the microgel film; statistically significant differences between groups can be seen in Tables S4 and S5. Two basic trends emerged; on films with a surface loss tangent greater than 1, cell area

showed a non-monotonic response where cell area increased until a surface loss tangent value ~1.1 and then decreased. However, on films with a surface loss tangent less than 1, cell area was highly variable and oscillated between cells with large spread areas and cells with low spread areas. This trend is also consistent with cell circularity where on films with a surface loss tangent greater than 1, cell circularity decreased until a surface loss tangent value of ~1.1 and then began to increase again. Likewise, on films with surface loss tangent values less than 1 the circularity was highly variable.

The variability in cell morphology on substrates with surface loss tangents lower than 1 could have implications in fibrotic responses. Previous studies have shown that as fibrosis progresses in healthy tissue, the viscoelasticity of the tissue decreases.[36–38] Furthermore, a vast degree of heterogeneity exists in fibroblasts undergoing fibrosis and myofibroblast differentiation.[39,40] These prior observed responses are in line with the observed heterogeneity in cellular morphology observed on composite substrates with surface loss tangent values less than 1.

The high degree of deviation on the composite substrates with surface loss tangents less than 1 could be due, at least in part, through cellular mechanotransduction signals occurring via nuclear deformation. Nuclear deformation has been shown to influence cell signaling by activating gene expression by decreasing the distance between chromosomes,[41] altering the rate of transport molecules through nuclear pores,[42] and/or by the supercoiling and bending of DNA and

altering the rates of DNA and RNA synthesis.[43] One way in which nuclear deformation can occur is through traction forces generated by the cells as they react and adjust to the mechanics of their environment.[44] As the traction forces generated by the cell increases, the nucleus will flatten and its area in a 2D focal plane will increase.[31] As the surface loss tangent of the composite substrate decreases, cells are able to generate larger traction forces, which will deform the nucleus as evident by the highly variable nucleus morphology observed on substrates with low surface loss tangent values. The variability in nucleus morphology then leads to different levels of mechanotransduction resulting in the higher degrees of variability in cellular morphology observed on the composite substrates with low surface loss tangent values. Interestingly, the trends in nuclear morphology did not seem to vary based on the stiffness of the underlying PA gel. Previous studies have linked substrate stiffness to driving nuclear morphology, such that nuclear area and aspect ratio increase, while nuclear circularity decreases on increasingly stiff substrates. However, our results suggest that it is possible to decouple this relationship as the observations related to nuclear morphology were similar across different stiffnesses but varied across different loss tangents. This opens up another avenue for study by which the importance of substrate loss tangent and its effect on nuclear morphology and subsequent cellular responses can be further explored.

To determine if changes in gene expression were seen on cells seeded on composite substrates, real-time quantitative PCR was performed on cells seeded on either a 2, 9, or 20 kPa substrate with a surface loss tangent of either 0.70, 0.81, 1.09, or 1.53 for α-SMA and CTGF, which are both markers for fibrotic responses and myofibroblastic differentiation. The PCR results similarly showed that the stiffness of the PA gel dictated the magnitude of the cellular responses, while the surface loss tangent of the microgel film modulated the trend of responses within each stiffness group. Initially, we hypothesized that α-SMA would increase with substrate stiffness in a similar manner to cellular area. However, our results for α-SMA expression showed a non-monotonic response based on the PA gel stiffness. Cells seeded on 20 kPa gels had the highest amounts of α-SMA expression, cells seeded on 9 kPa gels had the lowest amounts of α-SMA expression, and cells seeded on 2 kPa gels had intermediate amounts of α-SMA expression.

We believe that this non-monotonic response could be the result of differences in the internal tension of the fibroblast cells, which is influenced by the stiffness of the PA gel. Previous studies have linked α-SMA expression with internal cell tension, such that α-SMA expression increases when cells generate higher tensional forces.[45] Cells also attempt to match the mechanics of their microenvironment in a process known as tensional homeostasis with tensional forces increasing with increasing substrate stiffness.[46] However, studies have shown that this response plateaus, and cell stiffness will reach a maximum value even when the cells are seeded on much stiffer substrates, such as glass. For fibroblast cells, it has been shown that above a substrate stiffness of ~10 kPa, cell stiffness will reach its maximum of ~10 kPa and no longer increase, even if seeded on stiffer substrates, where stiffness was measured using AFM[47,48] This would indicate that

fibroblasts under normal tensional homeostatic conditions would have a stiffness value also ~10 kPa.

The three stiffnesses used in this study correspond to a value below the tensional homeostasis value of a fibroblast (2 kPa), a value approximately equal to the tensional homeostasis value of a fibroblast (9 kPa), and a value greater than the tensional homeostasis value of a fibroblast (20 kPa).[47,48] When fibroblasts seeded on a 2 kPa substrate attempt to undergo tensional homeostasis, the resulting internal stiffness value is lower than the homeostatic value, so α-SMA expression increases in order to increase the magnitude of the tensional forces that the cell can generate in an attempt to bring the cell back towards hemostasis. Fibroblasts seeded on 9 kPa substrates are able to match and reach their normal homeostatic internal tension values and thus become quiescent causing a decrease in α-SMA expression. Lastly, fibroblasts seeded on 20 kPa substrates have an over expression of α-SMA caused by an increase in contractility due to an abnormally stiff and fibrotic environment. This also corresponds to the morphology data collected with area increasing as the PA gel stiffness increases.

The analysis of α-SMA gene expression also indicated a potential non-monotonic response based on microgel film surface loss tangent where a surface loss tangent value of ~1.09 resulted in the lowest amounts of α-SMA expression. Although the data was not statistically significant, this data suggests a similar response to surface loss tangent as observed with substrate stiffness that warrants further investigation. In the same way that fibroblasts respond to changes in stiffness values above and below the homeostatic value for their internal cell stiffness, a similar response is likely occurring as a function of surface loss tangent. Biologically, cells with loss tangent values above 1.5 have been associated with diseased, malignant cell types as specifically seen in SW-13, A549, MCF-7, MDA-MB-231, and CaKi-1 cells.[49] Benign cells, however, were all seen to have loss tangent values lower than 1.5 but also higher than a loss tangent value of 1 as seen in NIH-3T3, MDCK-II, NMuMG, and MCF-10A cells.[49] Similarly, the loss tangent value of healthy epidermis ranges from 1.2–0.8[50] and the loss tangent value of health sheep aorta was found to be ~1.[51] These values all suggest that the homeostatic loss tangent value of a fibroblast cell is likely in the range of 0.8–1.2. The films used here have loss tangent values over the range of 1.8–0.7. To put these values in context, previous studies have reported blends of gelatin methacrylamide (GelMA) blends to have loss tangents[52] up to 0.23 and 0.2 mg/ml fibrin gels have loss tangents[53] of ~0.05. Our studies allow for probing cell responses higher than these previous reports.

Similar to stiffness, the viscoelasticity of tissue can change with fibrosis and with tissue damage. In the skin and other organs, scar tissue has been shown to decrease in viscoelasticity,[54] while damaged tissue increases in viscoelasticity compared to uninjured tissue.[55,56] The surface loss tangent values used in this study correspond to a viscoelasticity below the homeostatic value (0.70), in the same range as the homeostatic value (0.81 and 1.09), and above the homeostatic value (1.53) of fibroblast cells. On films with the lowest loss tangent values, α-SMA expression is higher due to overexpression caused by a high stiffness/low viscoelasticity environment similar to fibrotic scar
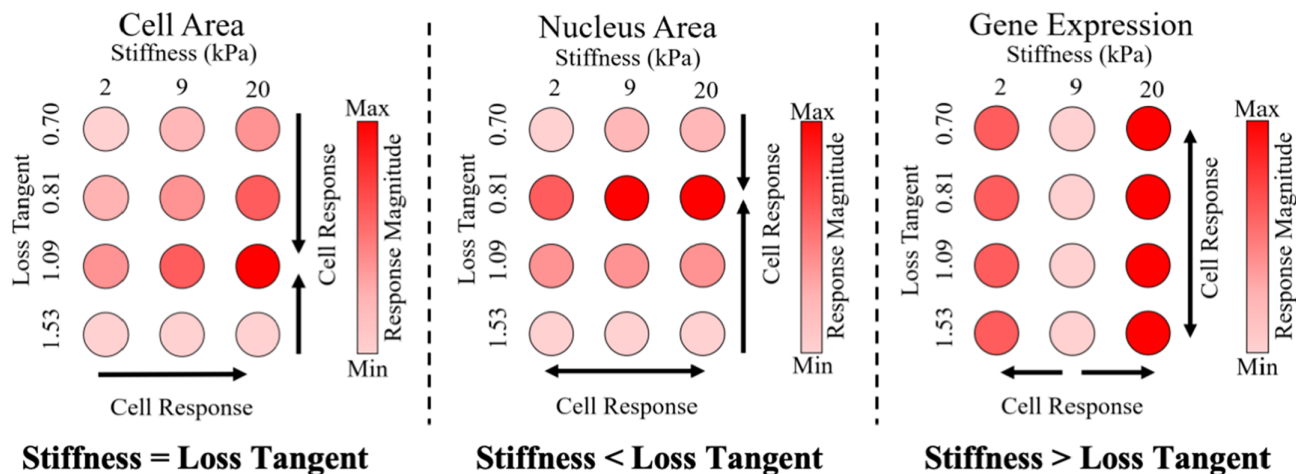
FIGURE 8 Summary of the effect of both substrate stiffness and surface viscoelasticity on cellular behavior: A summary of the combinatory effect that both substrate stiffness and surface viscoelasticity have on cellular behavior. Cellular area appeared to be modulated by both substrate stiffness and surface viscoelasticity as the highest areas were seen on composite substrate with the highest stiffnesses but intermediate loss tangent values. Nuclear area appeared to be modulated only by surface loss tangent and not substrate stiffness as the max nuclear area values were measured on substrates with a surface loss tangent of 0.81 irrespective of the substrate stiffness. Gene expression appeared to be modulated only by substrate stiffness and not by loss tangent as the rates of gene expression only changed across the different stiffness values and not the different loss tangent values

tissue. On the films with intermediate loss tangent values, α-SMA expression decreases due to the cells becoming quiescent due to the surface loss tangent values being in line with the homeostatic value of the fibroblast in its native environment. Finally, on films with high loss tangent values α-SMA expression increases. These results also match with the trends seen in cell area with the highest cell area occurring when the surface loss tangent value is ~1 and decreasing as the surface loss tangent increases to 1.5 while becoming variable on surface loss tangent values <1 due to the fibroblast populations undergoing fibrosis.

Similar to α-SMA expression, CTGF expression also showed a non-monotonic response in magnitude about substrate stiffness. Here, it was seen that cells seeded on both 2 and 20 kPa substrates had the highest rates of CTGF expression while cells seeded on the 9 kPa substrates has the lowest rates of CTGF expression. CTGF is known as a central mediator of tissue remodeling and fibrosis where higher levels of CTGF expression are linked to greater degrees of fibrosis and wound healing responses.[57] Specifically, CTGF is known to induce myofibroblast differentiation[58] and activates myofibroblasts to increase their rates of deposition and remodeling of ECM.[59–61] The same rationale for α-SMA's non-monotonic response in magnitude to substrate stiffness could contribute to the non-monotonic response seen with CTGF. However, CTGF expression did not seem to be directed by microgel film surface loss tangent, which indicates that surface loss tangent might not be an important mechanical cue for initiating CTGF signaling pathways.

However, these studies are not without limitations; staining for F-actin for visualization of the whole cell and imaging with confocal microscopy to allow for 3D reconstruction would allow for a more thorough understanding of the observed responses. Additionally, cell shape and size can dramatically change during cell division; use of a cell proliferative marker to clarify the influence of cell proliferation on

morphological differences would further clarify the responses. Future studies will utilize these analyses.

5 | CONCLUSIONS

Overall, we have shown that it is possible to create a composite substrate comprised of both microgel thin films and PA gels. We were able to create a material where both surface viscoelasticity and stiffness can be controlled independently of one another to obtain combinations of stiffness and viscoelasticity over a large range of physiologically relevant values. Through the use of this novel composite substrate (Figure 8), PA gel stiffness and microgel surface viscoelasticity was seen to be important in directing cellular morphology as the highest areas were measured on the stiffest substrate with intermediate surface loss tangent values. Nuclear morphology was seen to be more greatly impacted by surface loss tangent than substrate stiffness as the values were consistent across PA gel substrate stiffness while the highest values were measured on the intermediate loss tangent values. Lastly, gene expression was seen to be modulated by substrate stiffness and not as greatly by surface loss tangent as α-SMA and CTGF expression values were higher on the 2 and 20 kPa substrate but not statistically different across loss tangent values. This composite substrate also opens the possibility for further studying cellular processes while seeded on a substrate that more accurately mimics the mechanics of their native microenvironment to yield more accurate results in in vitro experimentation.

DATA AVAILABILITY STATEMENT

ORCID

Matthew B. Fisher ![ORCID icon] https://orcid.org/0000-0002-3212-0870
Ashley C. Brown ![ORCID icon] https://orcid.org/0000-0001-6995-1785

REFERENCES

1. Engler A, Bacakova L, Newman C, Hategan A, Griffin M, Discher D. Substrate compliance versus ligand density in cell on gel responses. *Biophys J*. 2004;86:617-628.
2. Engler AJ, Sen S, Sweeney HL, Discher DE. Matrix elasticity directs stem cell lineage specification. *Cell*. 2006;126:677-689.
3. Hadjipanayi E, Mudera V, Brown RA. Close dependence of fibroblast proliferation on collagen scaffold matrix stiffness. *J Tissue Eng Regen Med*. 2009;3:77-84.
4. Leipzig ND, Shoichet MS. The effect of substrate stiffness on adult neural stem cell behavior. *Biomaterials*. 2009;30:6867-6878.
5. Cox TR, Erler JT. Remodeling and homeostasis of the extracellular matrix: implications for fibrotic diseases and cancer. *Dis Model Mech*. 2011;4:165-178.
6. Hinz B. Matrix mechanics and regulation of the fibroblast phenotype. *Periodontol*. 2000;2013(63):14-28.
7. Cameron AR, Frith JE, Cooper-White JJ. The influence of substrate creep on mesenchymal stem cell behaviour and phenotype. *Biomaterials*. 2011;32:5979-5993.
8. Cameron AR, Frith JE, Gomez GA, Yap AS, Cooper-White JJ. The effect of time-dependent deformation of viscoelastic hydrogels on myogenic induction and Rac1 activity in mesenchymal stem cells. *Biomaterials*. 1857;2014:35-1868.
9. Chaudhuri O, Gu L, Klumpers D, et al. Hydrogels with tunable stress relaxation regulate stem cell fate and activity. *Nat Mater*. 2016;15: 326-334.
10. Chaudhuri O. Viscoelastic hydrogels for 3D cell culture. *Biomater Sci*. 2017;5:1480-1490.
11. Charrier EE, Pogoda K, Wells RG, Janmey PA. Control of cell morphology and differentiation by substrates with independently tunable elasticity and viscous dissipation. *Nat Commun*. 2018;9:449.
12. Mattei G, Cacopardo L, Ahluwalia A. Micro-mechanical viscoelastic properties of crosslinked hydrogels using the nano-epsilon dot method. *Materials*. 2017;10(8):889.
13. Cacopardo L, Guazzelli N, Nossa R, Mattei G, Ahluwalia A. Engineering hydrogel viscoelasticity. *J Mech Behav Biomed Mater*. 2019;89: 162-167.
14. Kwok MH, Li Z, Ngai T. Controlling the synthesis and characterization of micrometer-sized PNIPAM microgels with tailored morphologies. *Langmuir*. 2013;29:9581-9591.
15. Hashmi SM, Dufresne ER. Mechanical properties of individual microgel particles through the deswelling transition. *Soft Matter*. 2009;5:3682.
16. Sproul EP, Nandi S, Roosa C, Schreck L, Brown AC. Biomimetic microgels with controllable deformability improve healing outcomes. *Adv Biosyst*. 2018;2:2.
17. Joshi A, Nandi S, Chester D, Brown AC, Muller M. Study of poly(N-isopropylacrylamide-co-acrylic acid) (pNIPAM) microgel particle induced deformations of tissue-mimicking phantom by ultrasound stimulation. *Langmuir*. 2018;34:1457-1465.
18. Mihalko E, Huang K, Sproul E, Cheng K, Brown AC. Targeted treatment of ischemic and fibrotic complications of myocardial infarction using a dual-delivery microgel therapeutic. *ACS Nano*. 2018;12:7826-7837.
19. South AB, Whitmire RE, Garcia AJ, Lyon LA. Centrifugal deposition of microgels for the rapid assembly of nonfouling thin films. *ACS Appl Mater Interfaces*. 2009;1:2747-2754.
20. Hu X, Lyon LA. Thin films constructed by centrifugal deposition of highly deformable, charged microgels. *ACS Macro Lett*. 2015;4: 302-307.
21. Denisin AK, Pruitt BL. Tuning the range of polyacrylamide gel stiffness for mechanobiology applications. *ACS Appl Mater Interfaces*. 2016;8:21893-21902.
22. Chester D, Kathard R, Nortey J, Nellenbach K, Brown AC. Viscoelastic properties of microgel thin films control fibroblast modes of migration and pro-fibrotic responses. *Biomaterials*. 2018;185:371-382.
23. Lin YC, Tambe DT, Park CY, et al. Mechanosensing of substrate thickness. *Phys Rev E Stat Nonlinear Soft Matter Phys*. 2010;82:041918.
24. Tse JR, Engler AJ. Preparation of hydrogel substrates with tunable mechanical properties. *Curr Protoc Cell Biol*. 2010;47(1):10-16.
25. Gauthier J, Wu QV, Gooley TA. Cubic splines to model relationships between continuous variables and outcomes: a guide for clinicians. *Bone Marrow Transplant*. 2020;55:675-680.
26. Bachman H, Brown AC, Clarke KC, et al. Ultrasoft, highly deformable microgels. *Soft Matter*. 2018;2015:11-2028.
27. Saxena S, Spears MW Jr, Yoshida H, Gaulding JC, Garcia AJ, Lyon LA. Microgel film dynamics modulate cell adhesion behavior. *Soft Matter*. 2014;10:1356-1364.
28. Dahl KN, Ribeiro AJ, Lammerding J. Nuclear shape, mechanics, and mechanotransduction. *Circ Res*. 2008;102:1307-1318.
29. Buxboim A, Rajagopal K, Brown AEX, Discher DE. How deeply cells feel: methods for thin gels. *J Phys Condens Matter*. 2010;22:194116.
30. Hadden WJ, Young JL, Holle AW, et al. Stem cell migration and mechanotransduction on linear stiffness gradient hydrogels. *Proc Natl Acad Sci*. 2017;114:5647-5652.
31. Lovett DB, Shekhar N, Nickerson JA, Roux KJ, Lele TP. Modulation of nuclear shape by substrate rigidity. *Cell Mol Bioeng*. 2013;6:230-238.
32. Brown AC, Fiore VF, Sulchek TA, Barker TH. Physical and chemical microenvironmental cues orthogonally control the degree and duration of fibrosis-associated epithelial-to-mesenchymal transitions. *J Pathol*. 2013;229:25-35.
33. Davis JT, Wen Q, Janmey PA, Otteson DC, Foster WJ. Müller cell expression of genes implicated in proliferative vitreoretinopathy is influenced by substrate elastic modulus. *Investig Opthalmol Visual Sci*. 2012;53:3014-3019.
34. Yeung T, Georges PC, Flanagan LA, et al. Effects of substrate stiffness on cell morphology, cytoskeletal structure, and adhesion. *Cell Motil Cytoskeleton*. 2005;60:24-34.
35. Discher DE. Tissue cells feel and respond to the stiffness of their substrate. *Science*. 2005;310:1139-1143.
36. Yin M, Glaser KJ, Manduca A, et al. Distinguishing between hepatic inflammation and fibrosis with MR elastography. *Radiology*. 2017; 284:694-705.
37. Ebihara T, Venkatesan N, Tanaka R, Ludwig MS. Changes in extracellular matrix and tissue viscoelasticity in bleomycin-induced lung fibrosis. *Am J Respir Crit Care Med*. 2000;162:1569-1576.
38. Zhu Y, Zhang X, Zheng Y, et al. Quantitative analysis of liver fibrosis in rats with shearwave dispersion ultrasound vibrometry: comparison with dynamic mechanical analysis. *Med Eng Phys*. 2014;36:1401-1407.
39. Abraham DJ, Eckes B, Rajkumar V, Krieg T. New developments in fibroblast and myofibroblast biology: implications for fibrosis and scleroderma. *Curr Rheumatol Rep*. 2007;9:136-143.
40. Phan SH. Biology of fibroblasts and myofibroblasts. *Proc Am Thorac Soc*. 2008;5:334-337.
41. Berger SL. The complex language of chromatin regulation during transcription. *Nature*. 2007;447:407-412.
42. Feldherr CM, Akin D. The permeability of the nuclear envelope in dividing and nondividing cell cultures. *J Cell Biol*. 1990;111:1-8.
43. Thomas CH, Collier JH, Sfeir CS, Healy KE. Engineering gene expression and protein synthesis by modulation of nuclear shape. *Proc Natl Acad Sci USA*. 1972;2002:99-1977.

44. Kaminski A, Fedorchak GR, Lammerding J. The cellular mastermind (?)—mechanotransduction and the nucleus. *Prog Mol Biol Transl Sci*. 2014;126:157.

45. Shinde AV, Humeres C, Frangogiannis NG. The role of α-smooth muscle actin in fibroblast-mediated matrix contraction and remodeling. *Biochim Biophys Acta Mol Basis Dis*. 2017;1863:298-309.

46. Webster KD, Ng WP, Fletcher DA. Tensional homeostasis in single fibroblasts. *Biophys J*. 2014;107:146-155.

47. Solon J, Levental I, Sengupta K, Georges PC, Janmey PA. Fibroblast adaptation and stiffness matching to soft elastic substrates. *Biophys J*. 2007;93:4453-4461.

48. Gavara N, Chadwick RS. Determination of the elastic moduli of thin samples and adherent cells using conical atomic force microscope tips. *Nat Nanotechnol*. 2012;7:733-736.

49. Rother J, Noding H, Mey I, Janshoff A. Atomic force microscopy-based microrheology reveals significant differences in the viscoelastic response between malign and benign cell lines. *Open Biol*. 2014;4: 140046.

50. Kendall MA, Chong YF, Cock A. The mechanical properties of the skin epidermis in relation to targeted gene and drug delivery. *Biomaterials*. 2007;28:4968-4977.

51. Akhtar R, Graham HK, Derby B, et al. Frequency-modulated atomic force microscopy localises viscoelastic remodelling in the ageing sheep aorta. *J Mech Behav Biomed Mater*. 2016;64:10-17.

52. Bartnikowski M, Wellard R, Woodruff M, Klein T. Tailoring hydrogel viscoelasticity with physical and chemical crosslinking. *Polymers*. 2015;7:2650-2669.

53. Jansen KA, Bacabac RG, Piechocka IK, Koenderink GH. Cells actively stiffen fibrin networks by generating contractile stress. *Biophys J*. 2013;105:2240-2251.

54. Corr DT, Hart DA. Biomechanics of scar tissue and uninjured skin. *Adv Wound Care*. 2013;2:37-43.

55. Jan YK, Lung CW, Cuaderes E, Rong D, Boyce K. Effect of viscoelastic properties of plantar soft tissues on plantar pressures at the first metatarsal head in diabetics with peripheral neuropathy. *Physiol Meas*. 2013;34:53-66.

56. Chen Y, Qiu S, Wang C, Li X, Tang Y, Feng Y. Measurement of viscoelastic properties of injured mouse brain after controlled cortical impact. *Biophys Rep*. 2020;6:137-145.

57. Lipson KE, Wong C, Teng Y, Spong S. CTGF is a central mediator of tissue remodeling and fibrosis and its inhibition can reverse the process of fibrosis. *Fibrogenesis Tissue Repair*. 2012;5:S24.

58. Grotendorst GR, Rahmanie H, Duncan MR. Combinatorial signaling pathways determine fibroblast proliferation and myofibroblast differentiation. *FASEB J*. 2004;18:469-479.

59. Hishikawa K, Oemar BS, Nakaki T. Static pressure regulates connective tissue growth factor expression in human mesangial cells. *J Biol Chem*. 2001;276:16797-16803.

60. de las Heras N, Ruiz-Ortega M, Miana M, et al. Interactions between aldosterone and connective tissue growth factor in vascular and renal damage in spontaneously hypertensive rats. *J Hypertens*. 2007;25:629-638.

61. Chaqour B, Goppelt-Struebe M. Mechanical regulation of the Cyr61/CCN1 and CTGF/CCN2 proteins. *FEBS J*. 2006;273:3639-3649.

SUPPORTING INFORMATION

Additional supporting information may be found in the online version of the article at the publisher's website.